Volume 14-Issue 2 (2025)

Tạp chí Khoa học công nghệ Giao thông vận tải
Journal of Transportation Science and Technology
Trang tạp chí: https://tapchicongnghegtvt.vn

Effectiveness of Exhaust Gas Recirculation (EGR) system on reducing NOx pollutants on turbocharged Hydrogen engines

Huu Phuoc Nguyen[1], Duy Nam Ngo[2,3], Minh Hien Ngo[4], Van Chien Pham[2,3,*]

[1]*SDE Digital Technology Company Limited, Ho Chi Minh City, Vietnam*

[2]*Maritime Academy, University of Transport Ho Chi Minh City, Vietnam*

[3]*Artificial Intelligent in Transportation Research Group (AIT), University of Transport Ho Chi Minh City, Vietnam*

[4]*Bach Khoa Saigon College, Ho Chi Minh City, Vietnam*

**Corresponding author: chien.pham@ut.edu.vn*

Keywords:
EGR
Hydrogen engines
NOx pollutants

ABSTRACT

This paper presents a detailed analysis of a six-cylinder, 13.5 L turbocharged hydrogen (H_2) fueled spark ignition engine. The engine features direct injection and a low-pressure exhaust gas recirculation (LP EGR) loop. The objective is to demonstrate the engine's performance under various operating conditions using a basic engine control system integrated within the IFP-Engine library of Amesim software. The study successfully highlights the impact of different operating parameters on combustion efficiency and NOx emissions.

1. Introduction

Growing environmental concerns and stringent emission regulations have driven the exploration of emission-cutting technologies in the automotive industry. The 26th Conference of the Parties (COP26) in 2021 in the United Kingdom (UK) set a target of cutting net emissions by 40% (compared to 2008) by 2030 and to zero (net zero) by 2050 [1]. In this context, finding technical solutions to reduce engine emissions is essential for the internal combustion engine industry's survival. Emission reduction technologies for ICEs can be divided into three categories: (1) pre-treatment; (2) internal treatment; and (3) post-treatment [2].

To limit negative environmental impacts, the Environmental Protection Agency (EPA) of the United States has adopted Tier 1, Tier 2, and Tier 3 standards for NOx emissions. Since 2017, Tier 3 has been applied, which tightens the fleet average to 0.03 g/mile NOx. For on-

*Van Chien Pham. Maritime Academy, University of Transport Ho Chi Minh City, Vietnam; Artificial Intelligent in Transportation Research Group (AIT), University of Transport Ho Chi Minh City, Vietnam.
Email: chien.pham@ut.edu.vn

https://www.doi.org/10.55228/JTST.14(2).125-141
Recieved: February 5, 2025; Recieved in revised: March 13, 2025; Accepted: March 14, 2025
Available online: March 15, 2025
pISSN: 1859-4263; eISSN: 3030-4261

road heavy-duty diesel, the current EPA standard (since 2010) is 0.2 g/bhp-hr (grams per brake horsepower-hour) NOx [3].

The European Union has adopted Euro Emission Standards 1 to 6/7 (Euro 1 to 6/7). The current application is Euro 6, which limits the NOx to a maximum of 0.08 g/km NOx for diesel cars, and a maximum of 0.06 g/km NOx for petrol cars. Euro 7 is expected to be applied from 2025, which will tighten limits for both light and heavy-duty vehicles, applying to both tailpipe and real-world driving emissions (RDE) [4].

In the maritime sector, the International Maritime Organization (IMO) has adopted NOx emission regulations, namely IMO NOx Tiers – Tier I, II, and III, presented in Annex VI of MARPOL (the International Convention for the Prevention of Pollution from Ships). These "Tiers" define the maximum allowable NOx emissions, measured in grams per kilowatt-hour (g/kWh). IMO NOx regulations apply to marine diesel engines with a power output of more than 130 kW installed on ships. Since 2016, IMO Tier III has been applied, which limits NOx emissions from ships' main engines to 3.4 g/kWh for engine speeds of less than 130 rpm (revolutions per minute), and to 2.0 g/kWh for engine speeds of more than 2000 rpm [5].

Exhaust gas recirculation (EGR) is one of the effective emission-cutting internal treatment technologies. It was studied and applied to diesel engines to reduce NOx emissions from the 1970s. The studies show that the EGR impacts the combustion process of diesel engines on three aspects: (1) the thermal effect, (2) the dilution effect, and (3) the chemical effect. Ladommatos et al. [6] experimentally studied the thermal effect, the dilution effect, and the chemical effect of two mainly exhaust gas components (CO_2 and H_2O) of a diesel engine in 1997. The study showed the impact of EGR with various intake air temperatures on the combustion and emissions characteristics of the engine. Wang et al. [7] (2020) combined EGR with a Variable Turbocharger (VGT) to control the rate of EGR supplied to the engine based on intake pressure feedback and intake air mass flow rates. The experimental results pointed out that both NOx emissions, soot, and fuel consumption of the engine could be reduced by using this method. Yutaka Murata et al. [8] investigated the effect of high EGR rates on a common rail diesel engine in 2006. The research showed that, by optimizing the fuel multiple-stage injection, the NOx emissions characteristics of the engine could be improved.

Lattimore [9] (2016) investigated the effects of EGR on direct injection gasoline engines. The study mentioned that EGR is useful in both of these types of engines. Park and Bae [10] (2014) experimentally investigated the effect of EGR on a diesel engine. The research showed that NOx emissions could be significantly reduced by using this system. However, carbon monoxide (CO) and brake-specific fuel oil consumption (BSFC) increased accordingly. Roel Verschaeren also studied the effectiveness of EGR in reducing NOx emissions of medium-speed diesel engines. The study found that combining the EGR with the Miller cycle could reduce the NOx emissions to meet the International Maritime Organization (IMO) Tier III limits. Shen et al. [11] (2017) experimentally investigated the effects of LP EGR on a turbocharged gasoline direct injection (GDI) engine. The study reported that the LP EGR is useful in reducing NOx emissions from the engine at different speeds. Gorkem et al. [12] (2014) investigated the impact of EGR on a diesel engine which combined with steam injection. The study found that the system

reduced NOx emissions but increased CO and unburnt hydrocarbon (HC) emissions at the same time. Xiuxiu Sun [13] (2017) numerically investigated the emission characteristics of a diesel engine which used the EGR system by the computational fluid dynamics (CFD) analysis. The research reported a reduction of NOx emissions and brake specific fuel oil consumption (BSFC). Alegret et al. [14] (2015) used a nonlinear mean value model to develop an EGR model for diesel engines to reduce NOx emissions. Meanwhile, Zhu et al. [15] (2019) investigated the performance of SCR on reducing NOx emissions for a marine diesel engine. The above studies indicated that the NOx reduction mechanism of the EGR system is to reduce the peak temperature inside the cylinder by reducing the O_2 content in the engine intake air by recirculating a portion of the exhaust gas from the previous cycle (mainly containing CO_2 and H_2O) back into the engine intake port. The reduced O_2 content in the intake air lowers the temperature of the fuel combustion process, leading to a decrease in the combustion chamber temperature. The reduced combustion chamber temperature will limit the formation of thermal NO, which accounts for about 90% of NOx emissions from ICEs.

Hydrogen (H_2) has emerged as a potential candidate due to its zero-carbon emission characteristics. Using H_2 as an engine fuel is one of the effective pre-treatment emission-cutting Technologies [16]. As a non-toxic and carbon-free fuel, hydrogen (H_2) has been proven to be a clean and efficient fuel, especially in reducing carbon emissions [17]. When burning, H_2 emits less unburnt hydrocarbons (UHCs), particulate matter (PM), and no carbon-based emissions [18, 19]. H_2 had been shown to be suitable for use in internal combustion engines (ICEs) with near-zero engine-out emissions [20, 21].

Besides many advantages, H_2 has some technical disadvantages when used as a fuel in ICEs. The major problem is the high peak pressure inside engine cylinders, which could lead to knocking. The second thing is that its high ignition temperature led to a longer ignition delay (ID) time, which further increases the in-cylinder peak pressure, especially at high levels of H_2. High energy content resulting in high in-cylinder temperature, which leads to high thermal NOx emissions, is also a big problem with H_2. Additionally, backfire is another disadvantage. However, H_2 disadvantages could be solved if it is utilized as the primary fuel in dual-fuel (DF) engines instead of being used solely in compressed ICEs [16].

As shown in the literature review, applying the EGR system and H_2 fuel is a feasible solution for reducing engine emissions from diesel engines. This study tried to combine these two effective technologies to propose a solution to cut both NOx and carbon emissions which is very hard to achieve if using each solution only. This paper presents a detailed analysis of a six-cylinder hydrogen-fueled turbocharged spark-ignition engine equipped with direct injection and exhaust gas recirculation (EGR). This study calculates the engine's performance and NOx emissions under various operating conditions using the IFP-Engine library [22, 23]. Integrating the underlying engine control system, including the combustion controller and NOx model, is crucial to manage the engine operating conditions and optimize its performance. The insights gained from this study can contribute to developing more efficient and environmentally friendly H_2-powered engines.

2. Theoretical basis and Computational model

This study focuses on the analysis of the performance and emissions of a hydro-gen-fueled internal combustion engine (H_2-ICE) with a turbocharger system. The engine is modeled, and its parameters are tuned to optimize performance and minimize NOx emissions. The study uses the Long-Tail Wiebe combustion model and PI controllers corresponding to different powertrains to describe the engine operation and control.

This model allows calculating the evolution of the burned-fuel mass fraction (BMF) during the combustion process. Compared to the standard Wiebe law [24], it allows a better description of the slow combustion process, which is typical of modern small-sized high-performance engines, using high turbulence levels and high compression ratios.

In this approach, the beginning of the development of the BMF was based on the standard Wiebe law. The standard Wiebe's law is defined as [24]:

$$\mathbf{f_{wiebe}} = \mathbf{A_1}\frac{\mathbf{f_1+1}}{\mathbf{\Delta\theta}}.\left(\frac{\boldsymbol{\theta}}{\mathbf{\Delta\theta}}\right)^{\mathbf{f_1}}.\exp\left(-\mathbf{A_1}.\left(\frac{\boldsymbol{\theta}}{\mathbf{\Delta\theta}}\right)^{\mathbf{f_1+1}}\right) \quad (1)$$

Where A_1 and f_1 are the coefficients of Wiebe's law, respectively, $\Delta\theta$ is the angular time of the combustion process, and θ is the relative angular coordinate describing the combustion process.

The growth of the BMF is then modified to account for the end of the combustion process. Accordingly, the modified combustion law is defined as [25]:

$$\begin{aligned}\mathbf{f_{mod}} &= \frac{\exp\left(\mathbf{A_2}.\left(\frac{\boldsymbol{\theta}}{\mathbf{\Delta\theta}}\right)^{\mathbf{f_2}}\right).\frac{\mathbf{A_2 f_2}}{\mathbf{\Delta\theta}}.\left(\frac{\boldsymbol{\theta}}{\mathbf{\Delta\theta}}\right)^{\mathbf{f_2-1}}}{\exp\left(\mathbf{A_2}.\left(\frac{\boldsymbol{\theta}}{\mathbf{\Delta\theta}}\right)^{\mathbf{f_2}}\right)+\mathbf{1}} \\ &- \frac{\left(\exp\left(\mathbf{A_2}.\left(\frac{\boldsymbol{\theta}}{\mathbf{\Delta\theta}}\right)^{\mathbf{f_2}}\right)-\mathbf{1}\right).\exp\left(\mathbf{A_2}.\left(\frac{\boldsymbol{\theta}}{\mathbf{\Delta\theta}}\right)^{\mathbf{f_2}}\right).\frac{\mathbf{A_2 f_2}}{\mathbf{\Delta\theta}}.\left(\frac{\boldsymbol{\theta}}{\mathbf{\Delta\theta}}\right)^{\mathbf{f_2-1}}}{\left(\exp\left(\mathbf{A_2}.\left(\frac{\boldsymbol{\theta}}{\mathbf{\Delta\theta}}\right)^{\mathbf{f_2}}\right)+\mathbf{1}\right)^{\mathbf{2}}}\end{aligned} \quad (2)$$

Where:

$$\mathbf{A_2} = \frac{\log\left(-\frac{\mathbf{BMF_{switch}+1}}{\mathbf{BMF_{switch}-1}}\right)}{\left(\frac{\boldsymbol{\theta}_{\mathbf{switch}}}{\mathbf{\Delta\theta}}\right)^{\mathbf{f_2}}} \quad (3)$$

In the above equation, f_2 is a calibration parameter to fit the combustion time range, while the BMF_{switch} parameter represents the BMF curve value at which a discontinuous BMF slope is observed in the experimental curves; θ_{switch} is directly related to the BMF_{switch} value, it represents the corresponding transition angle and is calculated as follows:

$$\boldsymbol{\theta}_{\mathbf{switch}} = \mathbf{\Delta\theta}.\left(\frac{-\log(\mathbf{1-BMF_{switch}})}{\mathbf{A_1}}\right)^{\frac{\mathbf{1}}{\mathbf{f_1+1}}} \quad (4)$$

Note that the coordinate point (θ_{switch}, BMF_{switch}) on the BMF curve represents the point at which the BMF evolution transitions from the standard Wiebe law to the modified combustion model curve.

Finally, to ensure a smooth transition from one law to another, the BMF evolution is calculated as a combination of the above laws, according to the following equation [26]:

$$\begin{aligned}\mathbf{f_{wiebe_{mod}}} &= \frac{\mathbf{dBMF}}{\mathbf{d\theta}} \\ &= \frac{(\mathbf{f_{wiebe}}+\mathbf{f_{mod}})}{\mathbf{2}} \\ &+ \frac{(\mathbf{f_{wiebe}}-\mathbf{f_{mod}})}{\mathbf{2}}.\left[-\tanh\left(\frac{\boldsymbol{\theta}_{\mathbf{switch}}}{\mathbf{\Delta\theta}}.\frac{\mathbf{\Delta\theta}}{\mathbf{trans_{dur}}}.\mathbf{trans_{gain}}\right)\right]\end{aligned} \quad (5)$$

2.1. Combustion process and Heat release

The combustion process and heat release rate of the engine can be calculated using different methods as presented in the following subsections.

2.1.1. BMF central difference method

In this method, the heat release rate of combustion is calculated using the given central difference BMF. The mass of fuel burned is calculated using the following expression:

$$\left(\frac{\mathbf{dm_{fuel}}}{\mathbf{dt}}\right)_{\mathbf{combustion}} = \left(\frac{\mathbf{dBMF}}{\mathbf{dt}}\right).\mathbf{m_{ref}} \quad (6)$$

Where, $\left(\frac{\mathbf{dBMF}}{\mathbf{dt}}\right)$ is the value of the central derivative and m_{ref} is determined depending on the application and the ratio between the mass of fuel and the mass of air supplied to the engine (A/F equivalent ratios/AFRs/Air-to-Fuel equivalent ratios).

For spark ignition applications, m_{ref} is the mass of fuel present in the combustion chamber at the moment of ignition.

For compression ignition applications, m_{ref} is the mass of fuel injected specified at port 11 of the ENGBMFWIEBE01V01 model.

Using the change in mass of fuel and the LHV (Lower Heat Value) of the fuel under consideration (the fuel is represented here by the general formula $C_xH_yO_z$), the variation in the rate of heat release during combustion is calculated by:

$$\frac{\mathbf{dQ_{comb}}}{\mathbf{dt}} = -\mathbf{LHV}\cdot\left(\frac{\mathbf{dm_{fuel}}}{\mathbf{dt}}\right)_{\mathbf{combustion}} \quad (7)$$

2.1.2. Combustion heat release rate method

In this method, the growth of the combustion heat release rate is calculated directly from the combustion heat release rate provided by the input file. Then, the combustion mass flow rate is calculated using the following equation:

$$\left(\frac{\mathbf{dm_{fuel}}}{\mathbf{dt}}\right)_{\mathbf{combustion}} = -\frac{\mathbf{dQ_{comb}}}{\mathbf{dt}}.\frac{\mathbf{1}}{\mathbf{LHV}} \quad (8)$$

2.1.3. Wiebe Modeling Method

This method calculates the heat release rate of the combustion process using Wiebe's law. Wiebe's law can be used to calculate the evolution of the burned mass fraction during the combustion process. In this approach, the evolution of the burned mass fraction is determined using Wiebe's law in which the shape of the curve is assumed in advance [24]. The evolution of the burned mass fraction (BMF) is determined by equation (9) according to Wiebe's law:

$$\mathbf{f_{wiebe}} = \frac{\mathbf{dBMF}}{\mathbf{d\theta}} = \mathbf{A}.\frac{\mathbf{f+1}}{\mathbf{\Delta\theta}}.\left(\frac{\mathbf{\theta}}{\mathbf{\Delta\theta}}\right)^{\mathbf{f}}.\mathbf{exp}^{\left(-\mathbf{A}\left(\frac{\mathbf{\theta}}{\mathbf{\Delta\theta}}\right)^{\mathbf{f+1}}\right)} \quad (9)$$

Where, A and f are the coefficients of Wiebe's law. θ is the angle from the start of combustion and Δθ is the combustion time.

Knowing the mass fraction of fuel burned, the instantaneous heat released by the combustion process can be determined by:

$$\frac{\mathbf{dQ}}{\mathbf{d\theta}} = \frac{\mathbf{dBMF}}{\mathbf{d\theta}}.\mathbf{Q_{tot}} \quad (10)$$

Where, Q_{tot} is the total heat released during combustion.

Using the rate of heat release during combustion and the LHV of the fuel under consideration, the evolution of the fuel mass is calculated according to the following equation:

$$\left(\frac{\mathbf{dm_{fuel}}}{\mathbf{dt}}\right)_{\mathbf{combustion}} = -\frac{\mathbf{dQ_{comb}}}{\mathbf{dt}}.\frac{\mathbf{1}}{\mathbf{LHV}} \quad (11)$$

2.1.4. Long-Tail combustion Wiebe modeling method

In this method, the heat release rate of the combustion process is calculated by combining the formulas (1), (2), (3), (4), and (5).

Using the heat release rate during combustion and the LHV of the fuel under consideration, the growth of the fuel mass is calculated by equation (11).

When the heat release rate is known, using the air-to-fuel ratio (AFR), the increase in air mass is determined by:

$$\left(\frac{\mathbf{dm_{air}}}{\mathbf{dt}}\right)_{\mathbf{combustion}} = -\frac{\mathbf{AFR_{st}}}{\mathbf{LHV}}.\left(\frac{\mathbf{dQ_{comb}}}{\mathbf{dt}}\right) \quad (12)$$

Meanwhile, the increase in mass of the burned gas is calculated by the mass conservation equation according to the following expression:

$$\left(\frac{\mathbf{dm_{BG}}}{\mathbf{dt}}\right)_{\mathbf{combustion}} = -\left(\frac{\mathbf{dm_{fuel}}}{\mathbf{dt}}\right)_{\mathbf{combustion}} - \left(\frac{\mathbf{dm_{air}}}{\mathbf{dt}}\right)_{\mathbf{combustion}} \quad (13)$$

2.2. Heat transfer process

Heat transfer Q is calculated by correlations based on algorithms such as Eichel-berg, Annand, or Woschni, defined as follows:

2.2.1. Eichelberg equation

According to the Eichelberg equation, the amount of heat transferred is calculated as follows:

$$\mathbf{Q = 2.43 \cdot V_p \cdot S_\omega \cdot (T - T_\omega)\sqrt{PT}} \quad (14)$$

In which:

- P: is the pressure in the combustion chamber [Pa];
- T: is the temperature in the combustion chamber [K];
- Vp: is the mean speed of the piston [m/s];
- Sw: is the heat exchange surface of the cylinder wall [m2];
- Tw: is the temperature of the cylinder wall [K].

2.2.2. Annand equation

According to Annand equation, the amount of heat transferred is calculated as follows:

$$\mathbf{Q_{Annand} = h_{conv} \cdot (T_{gas} + T_w) \cdot S_w + \beta \cdot \sigma \cdot (T_{gas}^4 - T_w^4) \cdot S_w} \quad (15)$$

In which:

- h_{conv}: is the convection exchange coefficient calculated according to the function of combustion chamber geometry and the piston mean speed [W/m^2/K];
- T_{gas}: is the temperature in the combustion chamber [K];
- T_w: is the temperature of the cylinder wall [K];
- S_w: is the exchange surface of the cylinder wall [m^2];
- β: is the radiation coefficient (approximately 0.6) [-];
- σ: is the Stefan-Boltzmann constant; σ = 5,67e^{-8} [W/m^2/K^4].

2.2.3. Woschni equation

According to Woschni equation, the amount of heat transferred is calculated as follows:

$$\mathbf{Q = \frac{130 \cdot p^{0.8}}{T^{0.53} \cdot Bore^{0.2}} \cdot \left(C_1 \cdot V_p + C_2 \cdot \frac{V_0 \cdot T_1}{p_1 \cdot V_1} \cdot (p - p_0)\right)^{0.8} \cdot S_w} \quad (16)$$

$$\mathbf{V_p = 2 \cdot stroke \cdot omega} \quad (17)$$

In which:

- V_p: is the piston mean speed [m/s];
- stroke: is the piston stroke [m];
- omega: is the engine crankshaft rotation speed [rad/s];
- p: is the pressure in the combustion chamber [bar];
- T: is the temperature in the combustion chamber [K];
- C_1, C_2: are the first and second coefficients of the Woschni heat transfer model, they are determined in the eng_cyclephase2 utility according to the cycle phase (suction, compression, combustion, and exhaust);
- V_0: is the combustion chamber volume [m^3];
- p_1, T_1, V_1: are the pressure, temperature, and volume before combustion [bar, K,

m^3], respectively. They are also defined in the eng_cyclephase2 utility;

- p_0: is the intake air pressure [bar];
- S_w: is the wall surface area [m^2].

Accordingly, the eng_cyclephase2 utility determines the values of the first and second coefficients of the Woschni heat transfer model $C_{1woschni}$ and $C_{2woschni}$. Depending on the engine stroke, these values can change as shown below:

	TDC		Early ignition	TDC		TDC
Crankshaft Angle	0	180		360	540	720
Intake Valve	Open			Close		
Exhaust Valve		Close			Open	
C1woschni	C1woschni		C1woschni		C1woschni	
C2woschni	C2woschni			C2woschni	C2woschni	

Figure 1. $C_{1woschni}$ and $C_{2woschni}$ values according to crankshaft angle.

TDC in Figure 1 is the Top Dead Center, which is the end of the compression process, at which point the spark plug will emit a spark to ignite the mixture of air and fuel inside the combustion chamber, thereby starting the combustion process.

2.3. NOx Emissions

When the NOx emission model is activated, depending on the value of the parameter "application type", NOx emissions are calculated. For 'compression combustion' applications, the generation of NOx species is calculated using the *engbmfnox_IFPEN* utility. This utility calculates the mass change of NO, O_2, and N_2 components in the exhaust gas due to the following kinetic reaction:

$$\mathbf{O_2 + N_2 \rightleftharpoons 2NO} \tag{18}$$

The reaction rates ω_f and ω_b of the forward and reverse reactions, respectively, are calculated using the usual Arrhenius laws. To take into account the effect of the presence of combustion exhaust gas on NO production, the forward reaction rate is adjusted according to the following formula:

$$\boldsymbol{\omega_{f,b} = \omega_{f,b}(1 - bgrweightnox.fracgb)} \tag{19}$$

Allows access to the variation of the assumed species through the variable "mass NOx in combustion gas". In order to have consistent thermochemical properties of the gas in the combustion gas, the turbulent mass transfer from fresh gas to combustion gas is calculated using the *engbmfm* utility tool. This tool calculates the fresh gas mass transfer of the i^{th} species, *mgbentrainedot[i]*, into the combustion exhaust gas region due to turbulent entrainment according to the following model:

$$\mathbf{mgbentrainedot[i]} = -\frac{\mathbf{mgf[i]}}{\boldsymbol{\tau}} \tag{20}$$

Where, τ represents the characteristic mixing time of the turbulence and is calculated as follows:

$$\boldsymbol{\tau = CoeffGFGB \cdot Cdiss \cdot kspray^{0.5}/dinj} \tag{21}$$

The turbulent kinetic energy, "k_{spray}", is assumed to be generated entirely by the fuel injection flow rate, $\dot{m}_{inj}$, according to the following equation:

$$\dot{k}_{spray} = -C_{diss}\frac{k_{spray}^{1.5}}{d_{inj}} + \frac{C_{turb}}{m_{gas}}.\frac{\dot{m}_{inj}^3}{2\left(K_{inj}.n_{hole}\frac{\pi d_{inj}^2}{4}.\rho_l\right)^2} \tag{22}$$

Where, m_{gas} and ρ_l are the total mass of gas in the cylinder and the liquid density of the injected fuel, respectively.

For "Ignition" applications, the production of NOx species is calculated using the *engbmfzeldoreduced* utility, which allows access to the variation of the assumed species via the variable 'mass of NOx in combustion gas'. That is, this utility calculates the mass variation of NO, O_2, and N_2 species in the

combustion gas according to the Zeldovich reduction kinetic reaction. In this approach, the complete Zeldovich mechanism:

$$\mathbf{N_2 + O \rightleftharpoons NO + N} \quad (23)$$

$$\mathbf{NO + O \rightleftharpoons N + O_2} \quad (24)$$

The reaction rate of NO formation decreases to:

$$\frac{\mathbf{d[NO]}}{\mathbf{dt}} = \mathbf{c0_{NOx}.2.k_{1f}.[N_2].[O].}\left(\mathbf{1} - \frac{\mathbf{k_{1b}.k_{2b}.[NO]^2}}{\mathbf{k_{1f}.[N_2].k_{2f}.[O_2]}}\right) \Big/ \left(\mathbf{1} + \frac{\mathbf{k_{1b}.[NO]}}{\mathbf{k_{2f}.[O_2]}}\right) \quad (25)$$

Where k_{xy} denotes the reaction rate of the x^{th} reaction and the subscript y indicates whether the reaction rate refers to the forward (f) or reverse (b) reaction direction. The reaction rate is calculated using the usual Arrhenius law.

2.4. Mechanical transmission

The compressive force acting on the piston (F_{piston}) is calculated using the following expression:

$$\mathbf{F_{piston} = (P_{cyl} - P_{atmo}).A_{piston}} \quad (26)$$

Where:

- P_{cyl}: is the pressure in the combustion chamber;
- P_{atmo}: is the atmospheric pressure;
- A_{piston}: is the piston surface area.

The total volume of the combustion chamber is calculated by taking the total volume obtained by the piston displacement during the entire piston stroke and the dead volume, which is a parameter calculated from the other parameters of the model:

$$\mathbf{dv = \pi.B^2.\frac{R}{2.(rc - l)}} \quad (27)$$

In which:

$$\mathbf{rc = (V_d + V_c)/V_c} \quad (28)$$

With:

- **dv**: is dead volume;
- R: is crankshaft radius (1/2 piston stroke);
- rc: is the compression ratio;
- V_c: is combustion chamber volume;
- V_d: is the displacement volume created when the piston moves during its stroke.

3. Simulation of the engine

3.1. Engine configurations

The research engine is a 13.5 L, six-cylinder, turbocharged, spark-ignition engine fueled by hydrogen with direct injection and low-pressure exhaust gas recirculation (LP EGR) [22, 23, 25-29]. The main engine configurations are shown in Table 1.

Table 1. Main engine configurations.

Parameters	Values
Cylinder bore [mm]	130
Piston stroke [mm]	170
Connecting rod length [mm]	250
Compression ratio [-]	11
Combustion chamber height [mm]	2

The block diagram of the calculation process is shown in Figure 2.

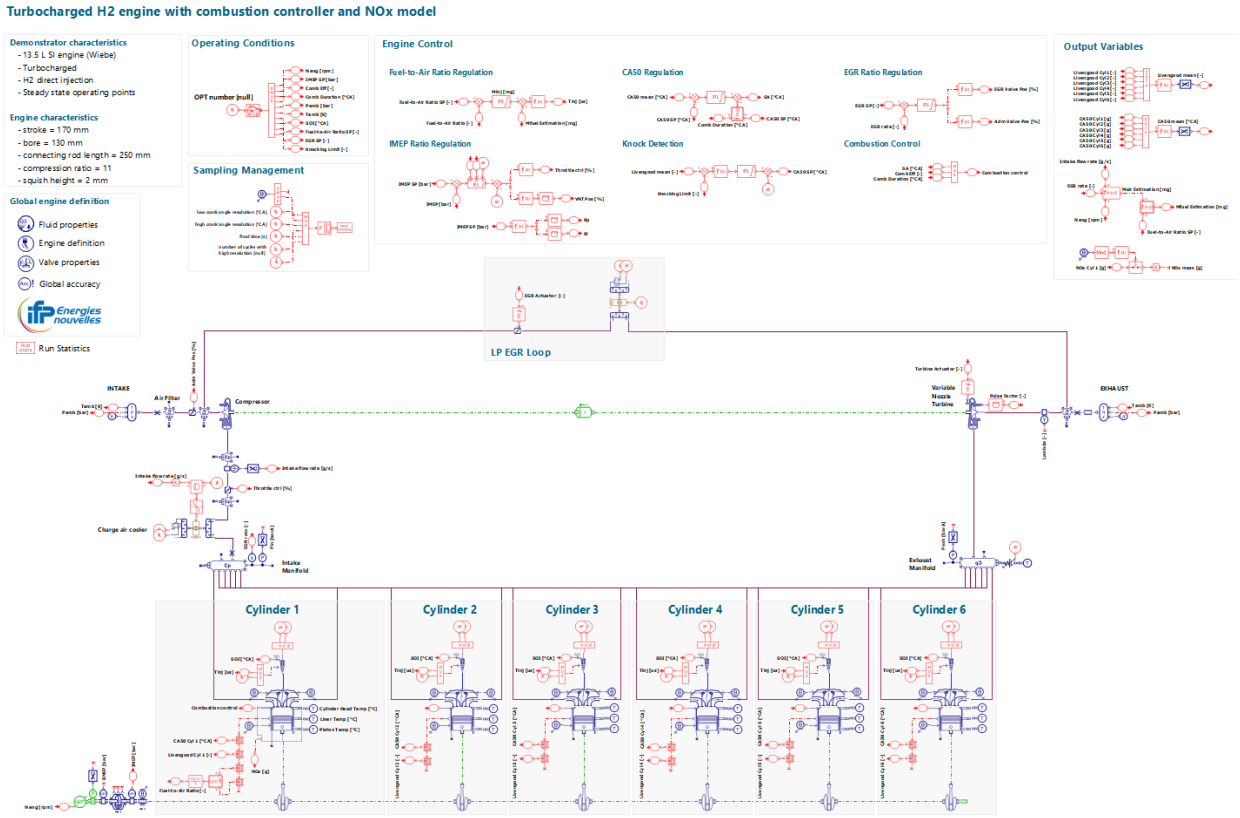

Figure 2. The block diagram of the calculation process.

3.2. Air intake and fuel injection system

The air intake and fuel injection system of the engine in the simulations is presented in Figure 3. The air intake system includes an air filter, an intake valve for controlling EGR, a compressor, a throttle, an intercooler, and a variable nozzle turbine. The LP EGR circuit comprises an EGR valve controller and a heat exchanger to manage the temperature of the recirculated gases. The direct injection system introduces H_2 gas into the combustion chamber using trapezoidal injection profiles [22-24, 30-33].

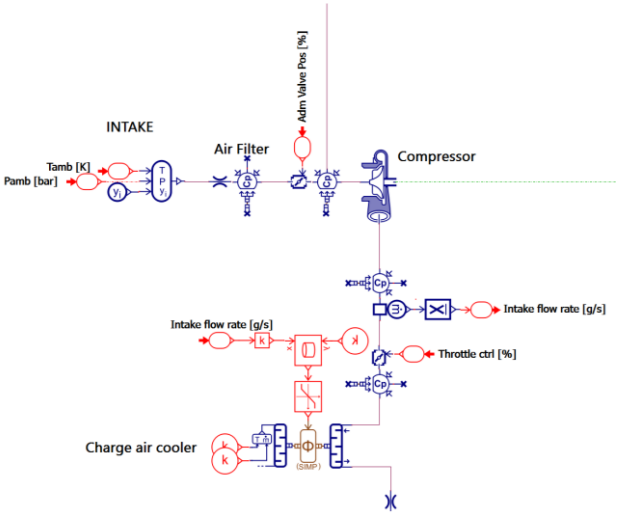

Figure 3. Air intake and fuel injection system.

3.3. In-cylinder combustion model in simulation software

3.3.1. Wiebe model

The combustion process is modeled using the Long-Tail Combustion Wiebe method. This model provides an analytical formula for the heat release process during combustion and

employs a two-zone approach to calculate phenomena involving fresh and burnt gases, such as knocking and NOx formation.

The Wiebe model is a widely used mathematical model for describing the combustion process in internal combustion engines. Developed by Ivan Wiebe in the mid-20th century, it has become a crucial tool for analyzing and simulating combustion. The Wiebe model describes the progression of the combustion reaction through a mathematical function, helping to predict changes in pressure and temperature within the combustion chamber. A schematic diagram for the Wiebe combustion model setting representation is shown in Figure 4.

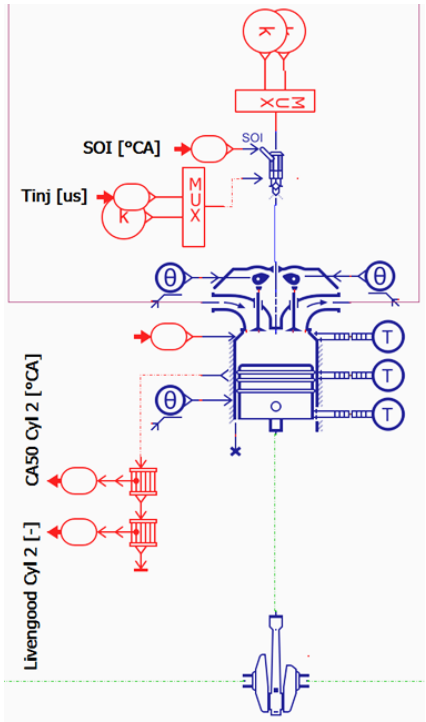

Figure 4. Combustion model representation.

The Long-Tail Combustion Wiebe model is an extended version of the basic Wiebe model, designed to provide a more detailed description of prolonged combustion, especially under varying operating conditions of H_2-ICE engines. It accounts for factors such as flame propagation and incomplete combustion, particularly in engines using alternative fuels like hydrogen [34, 35].

The general formula for the Wiebe model is expressed as follows:

$$\boldsymbol{\theta\%Burned = 1 - \exp\left(-a\left(\frac{\theta - \theta_0}{\Delta\theta}\right)^m\right)} \qquad (29)$$

Where:

- θ%Burned: is the percentage of fuel that has been burned;
- A: is the adjustment coefficient (usually related to the combustion rate);
- m: is the exponent of the Wiebe function (related to the shape of the combustion process);
- θ: is the crank angle;
- θ_0: is the start angle of the combustion process;
- Δθ: is the combustion duration (usually the difference in crank angle between the start and end of combustion).

The term Long-Tail refers to the extension of the tail of the heat distribution, indicating that a small portion of the fuel continues to burn after the majority of the combustion process has been completed. This is particularly important for fuels such as hydrogen, where the combustion process can extend longer compared to traditional fuels.

3.3.2. Advantage of the Long-Tail combustion Wiebe mode

- Higher Accuracy: Compared to the basic Wiebe model, the Long-Tail model provides a more accurate description of the combustion process, especially during the final stages;
- Versatile Applications: It is suitable for engine research using alternative fuels like hydrogen, where the combustion process can differ from traditional fuels;

- Detailed Analysis: It allows for in-depth analysis of temperature, pressure, and emissions throughout the combustion process, helping optimize engine performance and reduce NOx emissions.

3.3.3. Application in research

Within this study, the Long-Tail Combustion Wiebe model is used to simulate the combustion process in an H_2-ICE engine. This model aids in analyzing and predicting engine performance and NOx emissions under various operating conditions, while also supporting the development of engine control strategies to achieve optimal performance and emission reduction [36-43].

3.4. Engine Control Strategies

The engine control strategies is showed in Figure 5. The engine operates under eight different conditions, managed by proportional-integral (PI) controllers. These controllers adjust various actuators:

- Fuel injection quantity: Controls the equivalence ratio;
- Throttle position and variable nozzle turbine (VNT): Manages the indicated mean effective pressure (IMEP);
- EGR valve and intake valve position: Adjusts the EGR flow rate;
- Spark advance (SA): Controls the combustion phasing (CA50).

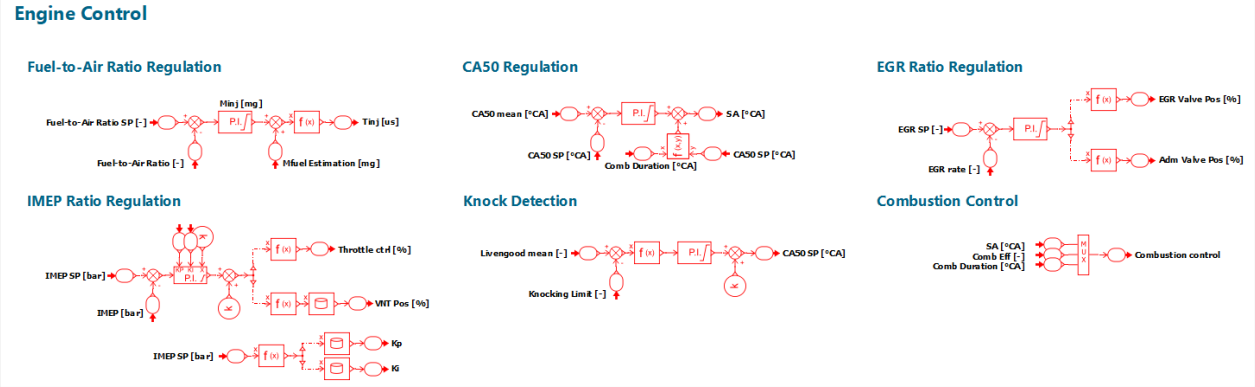

Figure 5. Engine Control System.

4. Results and Discussion

4.1. Engine performance

The engine performance is evaluated through eight operating points (OPT), determined by engine speed, IMEP, equivalence ratio, and EGR ratio as shown in Table 2. Each operating condition is tested until a steady state is reached, ensuring reliable data for analysis.

Table 2: Engine performance over time.

OPT	Batch	Engine speed (rpm)	IMEP (bar)	Equivalence ratio	EGR rate (%)
#1	Run 1	800	6	0.5	0
#2	Run 2	800	10	0.5	0
#3	Run 3	1200	22	0.45	0
#4	Run 4	1200	22	0.5	0
#5	Run 5	1200	22	0.5	5
#6	Run 6	1400	22	0.45	0
#7	Run 7	1400	22	0.5	0
#8	Run 8	1400	22	0.5	5

4.2. NOx Emissions

NOx (oxides of nitrogen) emissions from ICEs consist of thermal NOx, prompt NOx, and fuel NOx. It mainly refers to NO (nitric oxide)

and NO_2 (nitrogen dioxide). Thermal NOx is the most common type of NOx in high-temperature combustion conditions, especially in diesel engines. At very high temperatures condition (usually above 1800 K), N_2 and O_2 molecules react to form NOx. Conditions favouring thermal NOx are high flame temperatures, long residence combustion time, and high concentration of O_2. Prompt NOx forms early in the combustion process. It's generated by the reaction between N_2 in the intake air and hydrocarbon radicals (like CH, C, or other fragments) from the fuel. Conditions favouring prompt NOx are low-pressure and fuel-rich flames (e.g., in premixed combustion). Prompt NOx is usually a smaller contributor compared to thermal and fuel NOx. Fuel NOx comes from N_2 compounds already present in the fuel itself. When a fuel contains chemically-bound N_2 (common in coal, heavy fuel oils, ammonia, and some biofuels), combustion breaks these bonds and oxidizes the N_2 into NOx. The condition favouring fuel NOx is fuels with high nitrogen content (ammonia, coal, residual oils, etc.).

This study shows how NOx emissions are affected by engine operating conditions. Increasing the equivalence ratio from 0.45 to 0.5 leads to higher NOx emissions. However, the application of EGR significantly reduces NOx emissions. Additionally, higher engine speeds result in lower NOx emissions due to the reduced residence time of the combustion mixture at high temperatures.

This section will provide a more detailed explanation of the graphs related to NOx emissions under different operating conditions of the H_2-ICE.

Figures 6 and 7 below illustrate the relationship between engine speed and NOx emissions. It can be observed that as engine speed increases, NOx emissions decrease. This is due to the reduced residence time of the combustion mixture at high temperatures when engine speed increases, leading to a reduction in NOx formation.

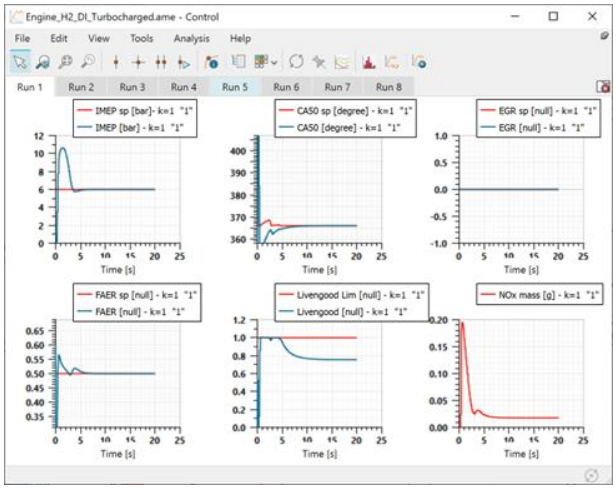

Figure 6. NOx emissions in simulation run 1.

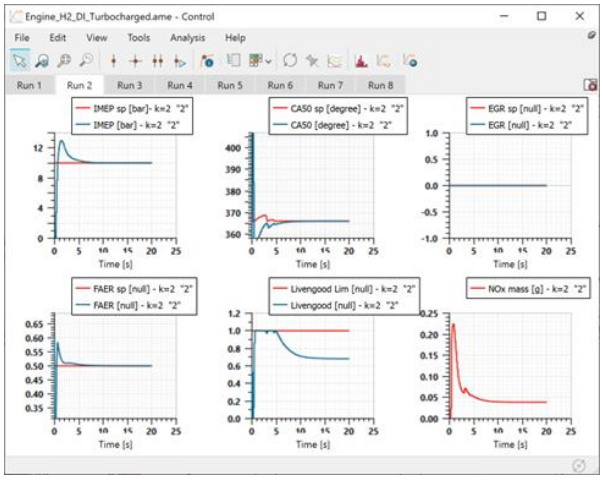

Figure 7: NOx emissions in simulation run 2.

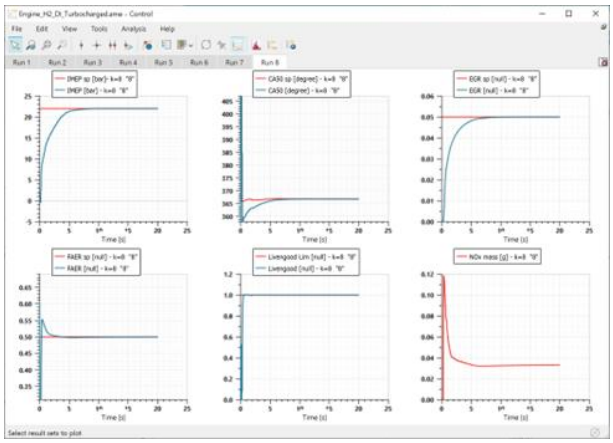

Figure 8: NOx emissions vs. engine speed.

Figure 8 illustrates the impact of the equivalence ratio on NOx emissions. As the equivalence ratio increases from 0.45 to 0.5, NOx emissions also rise. This is due to the excess fuel leading to higher temperatures in the combustion chamber, creating favorable conditions for NOx formation.

Figure 9 shows the effect of the EGR system on NOx emissions. As the EGR ratio increases, NOx emissions decrease significantly. This reduction occurs because exhaust gas recirculation lowers the combustion temperature, thereby reducing NOx formation.

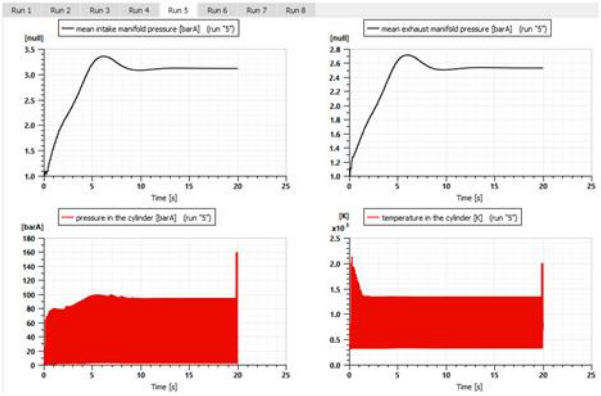

Figure 9: NOx emissions by equivalence ratio.

Figure 10 provides an overview of NOx emissions under various engine operating conditions. The operating points are defined by engine speed, IMEP, equivalence ratio, and EGR ratio. From the graph, it is evident that operating conditions greatly impact NOx emission levels. For instance, at higher engine speeds and lower equivalence ratios, NOx emissions are significantly lower.

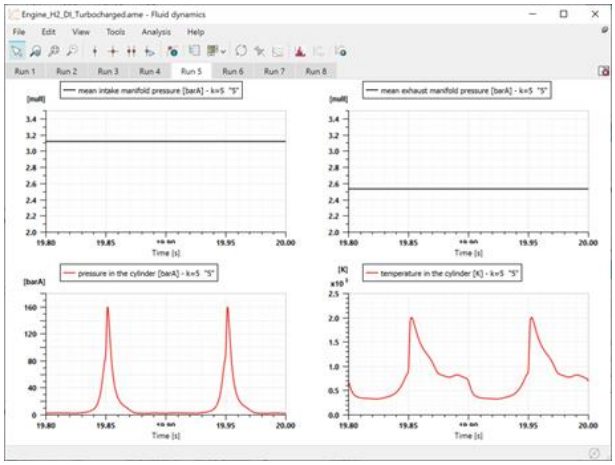

Figure 10: Impact of EGR on NOx emissions.

As shown in the Figure 11 below, by increasing the equivalence ratio from 0.45 to 0.5, the NOx specific emissions increase (engine calibration 1 vs 2). On the other hand, the introduction of EGR allows to reduce NOx as seen on engine calibration 3 compared to 2. It is also possible to observe that by increasing the engine speed NOx specific emissions are reduced, since the residence time of the burned gas mixture at high temperature is reduced (red dot vs blue square).

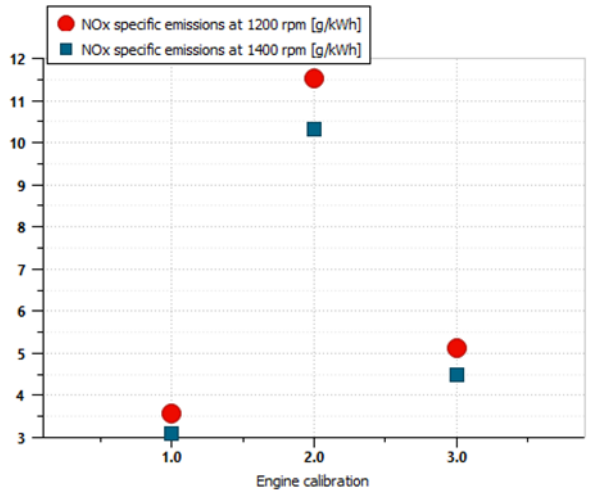

Figure 11: NOx emissions under various operating conditions.

4.3. Summary of NOx emissions analysis

The study shows that controlling parameters such as engine speed, equivalence ratio, and EGR ratio significantly impacts NOx emission levels in the H_2-ICE engine. A deeper

understanding of the relationship between these parameters and NOx emissions will aid in optimizing engine performance while minimizing harmful emissions.

Although the simulation results provide valuable insights into the role of EGR in reducing NOx emissions in turbocharged hydrogen engines, it is important to acknowledge that the current study is based solely on modeling using Siemens Amesim. As such, certain simplifications and idealized conditions - such as uniform gas mixing, constant turbocharger efficiency, and combustion delay assumptions - may not fully reflect the complexity of real-world engine operation.

To improve the reliability and applicability of the model, future work should include calibration and validation against experimental data obtained from hydrogen-fueled engine test benches. Parameters such as NOx formation, exhaust gas temperature, combustion stability, and CO emissions should be measured and compared to the simulation outcomes. This approach will allow for model refinement and ensure that EGR strategies can be implemented effectively in practical hydrogen engine systems.

5. Conclusions

Although the EGR strategy proves effective in reducing NOx emissions in turbocharged hydrogen engines, its implementation must be carefully calibrated. Excessive EGR may lead to incomplete combustion, thereby increasing CO emissions, and in certain cases, might also cause combustion instability or knocking phenomena. Future studies should evaluate these secondary effects under varying load and speed conditions to ensure optimal trade-offs between emission control and engine performance.

The study successfully illustrates the operating conditions and performance characteristics of a turbocharged six-cylinder H_2-fueled spark-ignition engine equipped with direct injection and EGR systems. Implementing a basic engine control system, including combustion control and NOx modeling, provides valuable insights into engine behavior across different operating points. The results highlight the importance of precise control over variables such as equivalence ratio, EGR ratio, and spark timing to prevent knocking and optimizing NOx emissions. These findings emphasize hydrogen's potential as a viable alternative fuel for heavy-duty engines, offering a pathway toward reduced carbon emissions and improved engine performance. Further research and development in this area could pave the way for broader adoption of hydrogen-powered engines in the automotive industry, contributing to more sustainable and cleaner transportation solutions.

Author Contributions

Huu Phuoc Nguyen: Data curation, Software, Investigation, Visualization, Reviewer response, Writing – original draft preparation. **Duy Nam Ngo:** Data curation, Data Analysis, Investigation, Validation. **Minh Hien Ngo:** Data curation, Data Analysis, Investigation. **Van Chien Pham:** Conceptualization, Methodology, Formal analysis, Investigation, Validation, Visualization, Supervision, Reviewer response, Writing – review and editing. All authors have read and agreed to the published version of the manuscript.

Conflict of Interest Disclosure and Copyright Disclaimer

The authors declare that there are no potential conflicts of interest arising from

this research and that the article has not been previously published.

Sharing data on demand

Data will be provided upon request.

Acknowledgements

The authors would like to thank Ho Chi Minh City University of Transport and the Artificial Intelligence in Transportation (AIT) Research Group for creating favorable conditions for the research process.

References

[1] U. Nations, "COP26 The Glasgow Climate Pact", [Online]. Available: https://webarchive.nationalarchives.gov.uk/ukgwa/20230401054904/https://ukcop26.org/ [Accessed: Feb 04, 2025].

[2] D. Woodyard, "Pounder's Marine Diesel Engines and Gas Turbines," ed: Elsevier/Butterworth-Heinemann, 2009.

[3] EPA, "What are the differences between Tier I and Tier II forms?", [Online]. Available: https://www.epa.gov/ [Accessed: April 17, 2025].

[4] E. K. w. A. Cantarelli, "Updating Euro emission standards (Euro 7)," European Parliamentary Research Service, 2023. [Online]. Available: https://www.europarl.europa.eu/RegData/etudes/BRIE/2023/740246/EPRS_BRI(2023)740246_EN.pdf.

[5] IMO. "International Convention for the Prevention of Pollution from Ships (MARPOL)." https://www.imo.org/en/about/Conventions/Pages/International-Convention-for-the-Prevention-of-Pollution-from-Ships-(MARPOL).aspx [accessed April 17, 2025].

[6] N. Ladommatos, S. Abdelhalim, H. Zhao, and Z. Hu, "The dilution, chemical, and thermal effects of exhaust gas recirculation on diesel engine emissions-Part 3: effects of water vapour," *SAE Technical Paper*, 0148-7191, 1997, doi: 10.4271/971659.

[7] Z. Wang, S. Zhou, Y. Feng, and Y. Zhu, "EGR modeling and fuzzy evaluation of Low-Speed Two-Stroke marine diesel engines," Science of the Total Environment, vol. 706, p. 135444, 2020, doi: 10.1016/j.scitotenv.2019.135444.

[8] Y. Murata et al., "Achievement of medium engine speed and load premixed diesel combustion with variable valve timing," *SAE Technical Paper*, 0148-7191, 2006, doi: 10.4271/2006-01-0203.

[9] T. Lattimore, "Combustion and emissions of a direct injection gasoline engine using EGR," University of Birmingham, 2016.

[10] Y. Park and C. Bae, "Experimental study on the effects of high/low pressure EGR proportion in a passenger car diesel engine," *Applied Energy*, vol. 133, pp. 308-316, 2014, doi: 10.1016/j.apenergy.2014.08.003.

[11] K. Shen, F. Li, Z. Zhang, Y. Sun, and C. Yin, "Effects of LP and HP cooled EGR on performance and emissions in turbocharged GDI engine," *Applied Thermal Engineering*, vol. 125, pp. 746-755, 2017, doi: 10.1016/j.applthermaleng.2017.07.064.

[12] G. Kökkülünk, A. Parlak, V. Ayhan, I. Cesur, G. Gonca, and B. Boru, "Theoretical and experimental investigation of steam injected diesel engine with EGR," *Energy*, vol. 74, pp. 331-339, Sep. 2014, doi: 10.1016/j.energy.2014.06.091.

[13] X. Sun, X. Liang, G. Shu, J. Lin, Y. Wang, and Y. Wang, "Numerical investigation of two-stroke marine diesel engine emissions using exhaust gas recirculation at different injection time," *Ocean Engineering*, vol. 144, pp. 90-97, Nov. 2017. 10.1016/j.oceaneng.2017.08.044.

[14] G. Alegret, X. Llamas, M. Vejlgaard-Laursen, and L. Eriksson, "Modeling of a large marine two-stroke diesel engine with cylinder bypass valve and EGR system," *IFAC-PapersOnLine*, vol. 48, no. 16, pp. 273-278, 2015, doi: 10.1016/j.ifacol.2015.10.292.

[15] Y. Zhu et al., "Performance optimization of high-pressure SCR system in a marine diesel. Part II: catalytic reduction and process," *Topics in Catalysis*, vol. 62, pp. 40-48, 2019. Available: https://link.springer.com/article/10.1007/s11244-018-1088-x [Accessed: Feb 04, 2025].

[16] V. C. Pham, J.-S. Kim, W.-J. Lee, and J.-H. Choi, "Effects of hydrogen mixture ratio and scavenging air temperature on combustion and emission characteristics of a 2-stroke marine engine," *Energy Reports*, vol. 9, pp. 195-216, 2023, doi: 10.1016/j.egyr.2022.11.207.

[17] S. Sharma and S. K. Ghoshal, "Hydrogen the future transportation fuel: From production to applications," *Renewable and sustainable energy reviews*, vol. 43, pp. 1151-1158, Mar. 2015, doi: 10.1016/j.rser.2014.11.093.

[18] N. Castro, M. Toledo, and G. Amador, "An experimental investigation of the performance and emissions of a hydrogen-diesel dual fuel compression ignition internal combustion engine," *Applied Thermal Engineering*, vol. 156, pp. 660-667, Jun. 2019, doi: 10.1016/j.applthermaleng.2019.04.078.

[19] T. Gatts, S. Liu, C. Liew, B. Ralston, C. Bell, and H. Li, "An experimental investigation of incomplete combustion of gaseous fuels of a heavy-duty diesel engine supplemented with hydrogen and natural gas," *International Journal of Hydrogen Energy*, vol. 37, no. 9, pp. 7848-7859, May. 2012, doi: 10.1016/j.ijhydene.2012.01.088.

[20] C. White, R. Steeper, and A. E. Lutz, "The hydrogen-fueled internal combustion engine: a technical review," *International Journal of Hydrogen Energy*, vol. 31, no. 10, pp. 1292-1305, Aug. 2006, doi: 10.1016/j.ijhydene.2005.12.001.

[21] H. An, W. Yang, A. Maghbouli, J. Li, S. Chou, and K. Chua, "A numerical study on a hydrogen assisted diesel engine," International journal of hydrogen energy, vol. 38, no. 6, pp. 2919-2928, Feb. 2013, doi: 10.1016/j.ijhydene.2012.12.062.

[22] ENGBMFWIEBE01V01, "Combustion Model Documentation," 2024.

[23] Siemens, "Turbocharged H2 Engine with Combustion Controller and NOx Model," 2023.

[24] N. Miyamoto, T. Chikahisa, T. Murayama, and R. Sawyer, "Description and analysis of diesel engine rate of combustion and performance using Wiebe's functions," *SAE transactions*, pp. 622-633, 1985. [Online]. Available: http://www.jstor.org/stable/44467700.

[25] R. R. Allen, "Multiport representation of inertia properties of kinematic mechanisms," Journal of the Franklin Institute, vol. 308, no. 3, pp. 235-253, Sep. 1979, doi: 10.1016/0016-0032(79)90115-7.

[26] Y. Zweiri, J. Whidborne, and L. Seneviratne, "Detailed analytical model of a single-cylinder diesel engine in the crank angle domain," *Proceedings of the Institution of Mechanical Engineers, Part D: Journal of Automobile Engineering*, vol. 215, no. 11, pp. 1197-1216, Nov. 2001, doi: 10.1243/0954407011528734.

[27] Institution of Mechanical Engineers, *Innovations in Fuel Economy and Sustainable Road Transport*, 1st ed. Oxford, UK: Woodhead Publishing, 2011. eBook ISBN: 9780857095879.

[28] C. A. R. Piedrahita and H. F. Q. Riaza, "Prediction of in-cylinder pressure, temperature, and loads related to the crank slider mechanism of IC engines: a computational model," *SAE Technical Paper* 2003-01-0728, Mar. 2003, doi: 10.4271/2003-01-0728.

[29] H.-Q. Do, L.-S. Tran, L. Gasnot, X. Mercier, and A. El Bakali, "Experimental study of the influence of hydrogen as a fuel additive on the formation of soot precursors and particles in atmospheric laminar premixed flames of methane," *Fuel*, vol. 287, p. 119517, Mar. 2021, doi: 10.1016/j.fuel.2020.119517.

[30] C.-Y. Lin and L.-W. Chen, "Comparison of fuel properties and emission characteristics of two- and three-phase emulsions prepared by ultrasonically vibrating and mechanically homogenizing emulsification methods," *Fuel*, vol. 87, no. 10-11, pp. 2154-2161, Aug. 2008, doi: 10.1016/j.fuel.2007.12.017.

[31] H. Gürbüz, H. Akçay, M. Aldemir, İ. H. Akçay, and Ü. Topalcı, "The effect of euro diesel-hydrogen dual fuel combustion on performance and environmental-economic indicators in a small UAV turbojet engine," *Fuel*, vol. 306, p. 121735, Dec. 2021, doi: 10.1016/j.fuel.2021.121735.

[32] M. S. Khan, I. Ahmed, M. I. b. A. Mutalib, S. Nadeem, and S. Ali, "Influence of H 2 O 2 on LPG fuel performance evaluation," *AIP Conference Proceedings*, vol. 1621, no. 1, pp. 763-768, Oct. 2014, doi: 10.1063/1.4898553.

[33] J. Liu, G. Li, and S. Liu, "Influence of ethanol and cetane number (CN) improver on the ignition delay of a direct-injection diesel engine," *Energy & fuels*, vol. 25, no. 1, pp. 103-107, 2011, doi: 10.1021/ef101231k.

[34] J. Liu and C. E. Dumitrescu, "Single and double Wiebe function combustion model for a heavy-duty diesel engine retrofitted to natural-gas spark-ignition," *Applied energy*, vol. 248, pp. 95-

103, Aug. 2019, doi: 10.1016/j.apenergy.2019.04.098.

[35] Y. Yeliana, C. Cooney, J. Worm, D. Michalek, and J. Naber, "Estimation of double-Wiebe function parameters using least square method for burn durations of ethanol-gasoline blends in spark ignition engine over variable compression ratios and EGR levels," *Applied thermal engineering*, vol. 31, no. 14-15, pp. 2213-2220, Oct. 2011, doi: 10.1016/j.applthermaleng.2011.01.040.

[36] A. Calle-Asensio, J. Hernández, J. Rodríguez-Fernández, M. Lapuerta, A. Ramos, and J. Barba, "Effect of advanced biofuels on WLTC emissions of a Euro 6 diesel vehicle with SCR under different climatic conditions," *International Journal of Engine Research*, vol. 22, no. 12, pp. 3433-3446, Mar. 2021, doi: 10.1177/14680874211001256.

[37] N. H. Razak, H. Hashim, N. A. Yunus, and J. J. Klemeš, "Reducing diesel exhaust emissions by optimisation of alcohol oxygenates blend with diesel/biodiesel," *Journal of Cleaner Production*, vol. 316, p. 128090, Sep. 2021, doi: 10.1016/j.jclepro.2021.128090.

[38] W. K. Hussam, M. N. Nabi, M. W. Chowdhury, M. E. Hoque, A. B. Rashid, and M. T. Islam, "Fuel property improvement and exhaust emission reduction, including noise emissions, using an oxygenated additive to waste plastic oil in a diesel engine," *Biofuels, Bioproducts and Biorefining*, vol. 15, no. 6, pp. 1650-1674, 2021, doi: 10.1002/bbb.2262.

[39] P. Appavu, J. Jayaraman, and H. Venu, "NOx emission reduction techniques in biodiesel-fuelled CI engine: a review," *Australian Journal of Mechanical Engineering*, vol. 19, no. 2, pp. 210-220, 2021, doi: 10.1080/14484846.2019.1596527.

[40] G. Goga et al., "Effects of ternary fuel blends (diesel-biodiesel-n-butanol) on emission and performance characteristics of diesel engine using varying mass flow rates of biogas," *Energy Sources, Part A: Recovery, Utilization, and Environmental Effects*, vol. 17, no. 1, pp. 6597-6610, 2021, doi: 10.1080/15567036.2021.1910754.

[41] C. B. Kumar, D. Lata, and D. Mahto, "Effect of addition of di-tert butyl peroxide (DTBP) on performance and exhaust emissions of dual fuel diesel engine with hydrogen as a secondary fuel," *International Journal of Hydrogen Energy*, vol. 46, no. 14, pp. 9595-9612, Feb. 2021, doi: 10.1016/j.ijhydene.2020.12.129.

[42] N. Seelam, S. K. Gugulothu, R. V. Reddy, and B. Burra, "Influence of hexanol/hydrogen additives with diesel fuel from CRDI diesel engine with exhaust gas recirculation technique: A special focus on performance, combustion, gaseous and emission species," *Journal of Cleaner Production*, vol. 340, p. 130854, Mar. 2022, doi: 10.1016/j.jclepro.2022.130854.

[43] G. Di Blasio, R. Ianniello, and C. Beatrice, "Hydrotreated vegetable oil as enabler for high-efficient and ultra-low emission vehicles in the view of 2030 targets," *Fuel*, vol. 310, p. 122206, Feb. 2022, doi: 10.1016/j.fuel.2021.122206.